RSC Advances

PAPER

View Article Online
View Journal | View Issue

Check for updates

Cite this: *RSC Adv.*, 2018, **8**, 29928

Design and controllable synthesis of ethylenediamine-grafted ion imprinted magnetic polymers for highly selective adsorption to perchlorate† ‡

Haoyu Shen, *[a] Meina Sun,[b] Meiqin Hu[a] and Jinjin Cheng[a]

Received 18th July 2018
Accepted 17th August 2018

DOI: 10.1039/c8ra06085a

rsc.li/rsc-advances

A series of ethylenediamine-grafted ion imprinted magnetic polymers (Fe_3O_4@IIPs) were synthesized *via* ultrasonic assisted suspension polymerization with perchlorate (ClO_4^-) as an ion imprinting template. They were characterized by XRD, EA, VSM, FTIR and XPS and applied as adsorbents for ClO_4^- removal from aqueous solutions. The effects of the usage amount of crosslinking agent divinylbenzene (DVB) used for preparation on the structure and the adsorptive performance of Fe_3O_4@IIPs were investigated. The results show that the Fe_3O_4@IIPs have an average size of 200–800 nm, which increases with the increase of the amount of DVB from 0 to 2 g during the preparation process. The saturation magnetization intensities are at 35.6–42.8 emu g^{-1}, which decrease with the increase of the usage amount of DVB. The addition of DVB is beneficial to the formation and stability of the ion imprinted cavity of Fe_3O_4@IIPs. The effects of the solution pH value, initial concentration of ClO_4^-, and adsorption time on the adsorption properties of ClO_4^- in aqueous solutions were investigated. The results show that the adsorption capability is affected significantly by solution pH value and reaches the maximum adsorption capacity at pH 3.0. The best adsorption capacity and selectivity of Fe_3O_4@IIPs to ClO_4^- can be obtained when the usage amount of DVB is at 0.5 g for synthesis. The adsorption mechanisms might include both ion exchange and electrostatic interaction. The isothermal adsorption curves mainly obey the Langmuir model with the theoretical maximum adsorption capacities ($q_{m,c}$) at 76.92–111.1 mg g^{-1} and the experimental maximum adsorption capacities ($q_{m,e}$) at 75.7–108.9 mg g^{-1}, respectively, which are much higher than those of the non-ion imprinted material (Fe_3O_4@NIP, $q_{m,NIP}$: $q_{m,c}$ at 60.61 mg g^{-1} and $q_{m,e}$ at 59.0 mg g^{-1}). The adsorption kinetic studies show that the adsorption processes reach equilibrium within 10 min and the kinetic data are well fitted to the pseudo-second-order model. There is almost no interference by the coexisting anions for the selective adsorption of ClO_4^-, with a imprinting factor (α) at 1.8, and selectivity factor (β) larger than 5.9 for several kinds of common co-existing anions, respectively. The Fe_3O_4@IIPs are ideal candidates for removal of ClO_4^- from aqueous solution.

1. Introduction

Perchlorate (ClO_4^-) is a newly emerging, persistent environmental pollutant with high water solubility, mobility and stability, which poses a potential health threat to humans.[1] Because of its strong oxidative property, ClO_4^- is often used as a safe oxidant, and has been widely used in military manufacturing and industrial production, such as in solid rocket fuels, missiles, explosives, pyrotechnics, fireworks, *etc.*[2,3] ClO_4^- has also been widely used in clinical treatment of hyperthyroidism caused by immune system defects and clinical examination of thyroxine secretion, *etc.*[4] Since the charge and ionic radius of ClO_4^- are very close those of the iodine ion (I^-), ClO_4^- has been found to inhibit the uptake of iodine and disturb the synthesis of the thyroid hormone, which would affect the development of the central nervous system in newborns and induce thyroid cancer.[5]

Because of its high water solubility and stability, the degradation of ClO_4^- in the natural environment needs several decades or even longer.[5] Conventional treatment processes, such as coagulation, precipitation, filtration and disinfection, cannot remove ClO_4^- efficiently.[6,7] Current technologies for ClO_4^- removal from drinking water and groundwater include

---

[a] *Ningbo Institute of Technology, Zhejiang University, Ningbo, 315100, China. E-mail: hyshen@nit.zju.edu.cn; Tel: +86-574-88130130*

[b] *Greentown Agricultural Testing Technology Co., Ltd, Hangzhou, 310052, China*

† Dedicated to Prof. Dai-Zheng Liao on the occasion of his 80th birthday.

‡ Electronic supplementary information (ESI) available. See DOI: 10.1039/c8ra06085a

adsorption,[8,9] ion exchange,[10,11] chemical reduction[12–14] bioremediation,[14,15] *etc.*

An ion imprinted polymer (IIP)[16–18] is able to recognize ions whilst keeping the unique virtues of molecular imprinting polymers (MIP), *i.e.*, structure predictability, recognition specificity and application universality. Owing to special coordination or electrostatic interactions, IIPs are generally compatible with aqueous media and have advantages over most MIPs.[16] IIPs can achieve effective identification of water-soluble ions. However, centrifugation or long-time subside is still needed for the separation of the IIPs from the post-adsorption solution, which is time-consuming and inefficient. Recently, functional group grafted nano-magnetic particles (FNMPs) have attracted greats attention because of their unique magnetic and structural properties.[19–24] It would be desirable if the high selectivity, good adsorptive efficiency and fast magnetic separation were associated by grafting the IIPs on the surface of the FNMPs *via* such a three-in-one strategy. The obtained material would be expected to not only retain the high selective recognition of IIPs to the target ion, but also to achieve the goal of high adsorption capacity, as well as fast removal of the contaminant.

Herein, in this work, we report the design and successful synthesis of a serial of core–shell microspheres ion imprinted magnetic polymers (Fe_3O_4@IIPs), by using ClO_4^- as the template. Their applications as adsorbents for ClO_4^- removal from aqueous solutions were studied. By varying the usage amount of DVB during the preparation procedure, the structure and adsorption properties on ClO_4^- were tuned. Based on the investigation of the effects of solution pH values and common co-existing anions on the adsorption properties, adsorption thermodynamic, kinetic parameters, as well as comparing with that of the non-ion imprinted magnetic polymer composite (Fe_3O_4@NIP), the adsorption mechanism was intensively studied. The results show that the Fe_3O_4@IIPs are ideal candidates for adsorption and removal ClO_4^- from aqueous solution.

2. Experimental

2.1. Materials

Ferric chloride ($FeCl_3 \cdot 6H_2O$), sodium acetate (NaAc), ethylene glycol (EG), potassium perchlorate ($KClO_4$), were analytical grade, and purchased from Sinopharm Chemical Reagent Co., Ltd. ethylenediamine (EDA), styrene (St), divinylbenzene (DVB) and glycidylmethacrylate (GMA) were supplied by Aladdin Chemical Reagent Co., Ltd. (Shanghai, China) and purified by vacuum distillation. Benzoyl peroxide (BPO) was purchased from J&K Chemical (99%) and used as an initiator without further purification. Distilled water was used to prepare all the solutions. 0.1 mol L^{-1} HCl and 0.1 mol L^{-1} NaOH solutions were used for pH adjustment.

2.2. Synthesis of nFe_3O_4@IIPs

The overall preparation of ClO_4^--imprinted magnetic polymers (nFe_3O_4@IIPs) is depicted in Scheme 1. 4 kinds of nFe_3O_4@IIPs, as listed in Table 1, were prepared by the following steps *via* suspension polymerization and surface imprinting technique. The preparation procedure of nFe_3O_4@IIP-D0.5-G8 (no. 2) was taken as an example for discussion.

Firstly, the nano-Fe_3O_4 (nFe_3O_4, no. 6) was produced using a polyol-media one-pot solvothermal method (Scheme 1(a)). 4.0 g of $FeCl_3 \cdot 6H_2O$, and 12.0 g of NaAc were dissolved in 120 mL ethylene glycol (EG). This solution was stirred vigorously at room temperature for 10 min to form a stable orange solution and then transferred to a Teflon-lined autoclave and heated at 180 °C for 8 h. After the autoclave cooled to room temperature, the resulting nFe_3O_4 was isolated under magnetic field and washed with water and ethanol to remove redundant reagents and impurities. The as-prepared nFe_3O_4 was dried in a vacuum oven at 60 °C for 12 h and stored in a sealed bottle for further use.

Then, the ClO_4^--template solution was prepared (Scheme 1(b)). 5 mL of 0.2 mol L^{-1} EDA ethanol solution and 8 mL of 0.2 mol L^{-1} GMA ethanol solution were mixed and stirred at room temperature for 30 min, followed by adding 10 mL of 0.2 mol L^{-1} $KClO_4$ ethanol solution dropwisely, and stirred at room temperature for another 2 h, to obtain the ClO_4^--templated functional monomer solution at the concentration of 0.1 mol L^{-1} (calculated based on the ClO_4^-).

Afterward, nFe_3O_4@IIPs was prepared by dispersive polymerization (Scheme 1(c)). 1.0 g of nFe_3O_4 was dispersed 25 mL ethanol under ultrasonication, then the above obtained 20 mL of ClO_4^--template solution, and 10 mL 0.2 mol L^{-1} of St ethanol solution, and 0.5 g DVB were added accordingly. Finally, 0.1 g of benzoyl peroxide (BPO) dissolved in 25 mL ethanol was added dropwisely under vigorously stirring. The mixture was continuously reacted at 80 °C for 3 h. The template ion, ClO_4^-, was cleaned with 0.5 mol L^{-1} NaOH ethanol solution for several times under ultrasound until ClO_4^- could not be detected by photometric method.[25] Then protonated by 0.5 mol L^{-1} HAc ethanol solution to obtain the final nFe_3O_4@IIP, named as nFe_3O_4@IIP-D0.5-G8. The as-prepared nFe_3O_4@IIP-D0.5-G8 were washed with water three times, dried in a vacuum oven at 60 °C and stored in a sealed bottle for further use.

Other 3 kinds of nFe_3O_4@IIPs (no. 1, 3, and 4) were synthesized with different usage amount of DVB at 0 g, 1 g, and 2 g, respectively, listed in Table 1. In parallel, the non-imprinted magnetic polymer (nFe_3O_4@NIP-D0.5-G8, no. 5) was synthesized almost the same procedures described above without the addition of the templates.

2.3. Characterization

The morphology and dimensions of as-prepared nFe_3O_4@IIPs were obtained on a Hitachi H-7650 transmission electron microscopy (TEM) (Hitachi, Japan) at an accelerating voltage of 75 kV. The magnetic properties of magnetic particles were measured using a vibrating sample magnetometer (VSM, Lake Shore 7410). Powder X-ray diffraction (XRD) patterns were collected on an X-ray diffractometer (Bruker D8 Advance) with CuKα radiation at $\lambda = 0.154$ nm operating at 40 kV and 40 mA. The content of Fe_3O_4 in each of nFe_3O_4@IIPs was calculated from the amount of leached Fe, which was measured by using a spectrophotometer (722, Shanghai, China) according to the

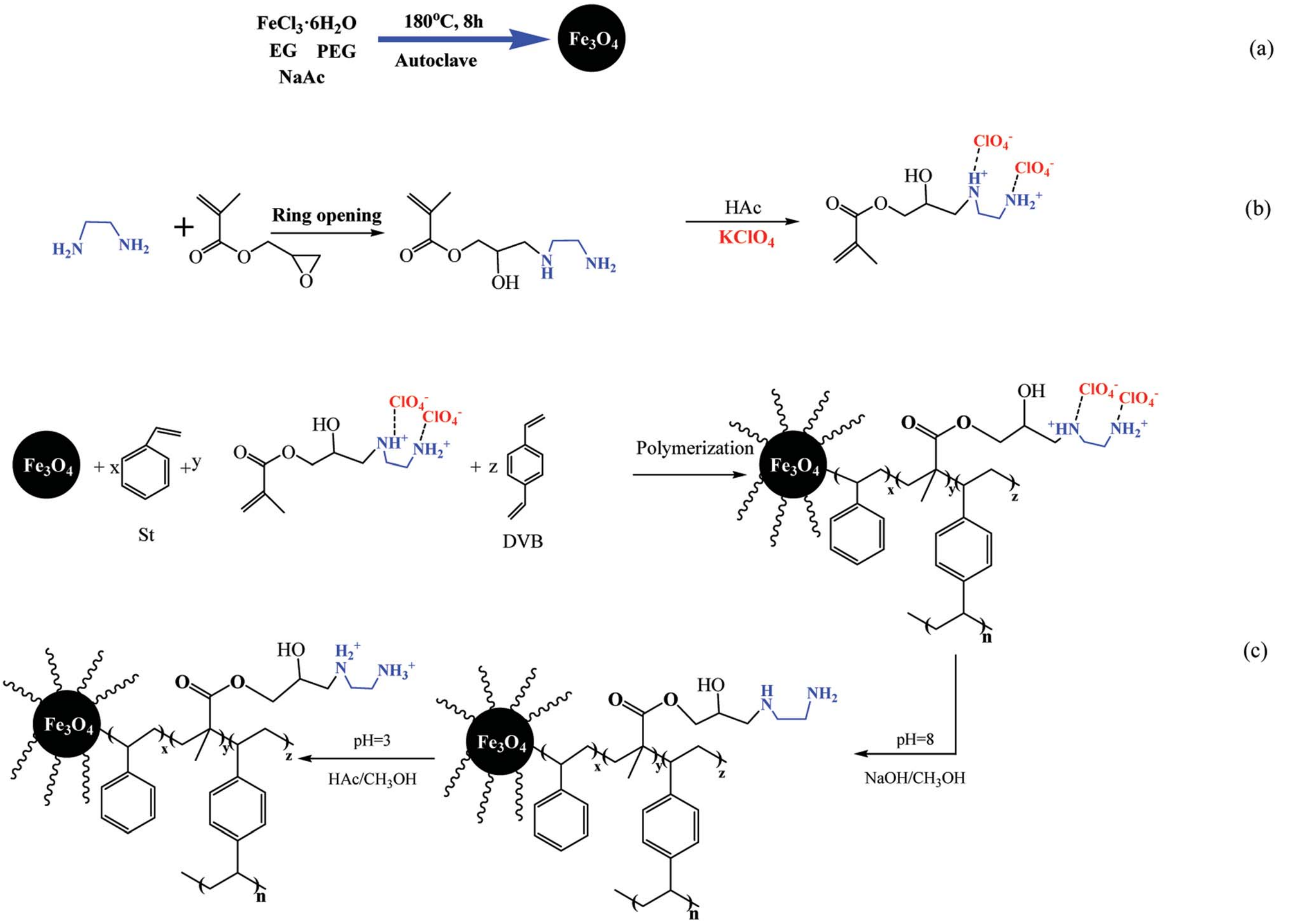

Scheme 1 Schematic procedure of preparation of nFe_3O_4@IIP.

standard colorimetric method[26] after digesting nFe_3O_4@IIPs in 12 mol L^{-1} HCl solution. The elementary analysis results of the nitrogen contents in nFe_3O_4@IIP were measured using an elementary analysis (EA, Thermo Fisher Flash-1112). Fourier Transform Infrared spectrometer (FTIR, Thermo Nicolet, USA) were applied for characterization.

2.4. Adsorption experiments

Batch adsorption experiments were carried out in 150 mL stoppered flasks, each of which contained 25 mL of $KClO_4$ solution. A 20 mg amount of adsorbents was added into each flask and shaken at 180 rpm in a thermostatic shaker. The solution pH was adjusted by 0.1 mol L^{-1} HCl or 0.1 mol L^{-1} NaOH solution. The $KClO_4$ concentration in the supernatant was measured by colorimetric method.[25] According to the ClO_4^- concentrations before and after adsorption, the equilibrium adsorption capacity (q, mg g^{-1}) of ClO_4^- bound to the nFe_3O_4@IIP is calculated using eqn (1):[27]

$$q = \frac{(C_0 - C_e)V}{m} \tag{1}$$

where C_0 and C_e represent the initial solution concentration and the equilibrium concentration of ClO_4^- (mg L^{-1}), V is the

Table 1 Content of Fe_3O_4, N, saturation moments and average diameter of nFe_3O_4@IIP

No.	Adsorbents	Content of Fe_3O_4 (%)	Content of N (mmol g^{-1})	Saturation moments (emu g^{-1})	Average diameter (nm)
1	nFe_3O_4@IIP-D0-G8	41.5	7.82	42.8	200
2	nFe_3O_4@IIP-D0.5-G8	39.5	7.45	40.5	400
3	nFe_3O_4@IIP-D1-G8	37.6	7.22	38.7	500
4	nFe_3O_4@IIP-D2-G8	35.4	7.08	35.6	400–800
5	nFe_3O_4@NIP-D0.5-G8	39.8	7.38	40.8	200–600
6	nFe_3O_4	96.8	—	72.8	200

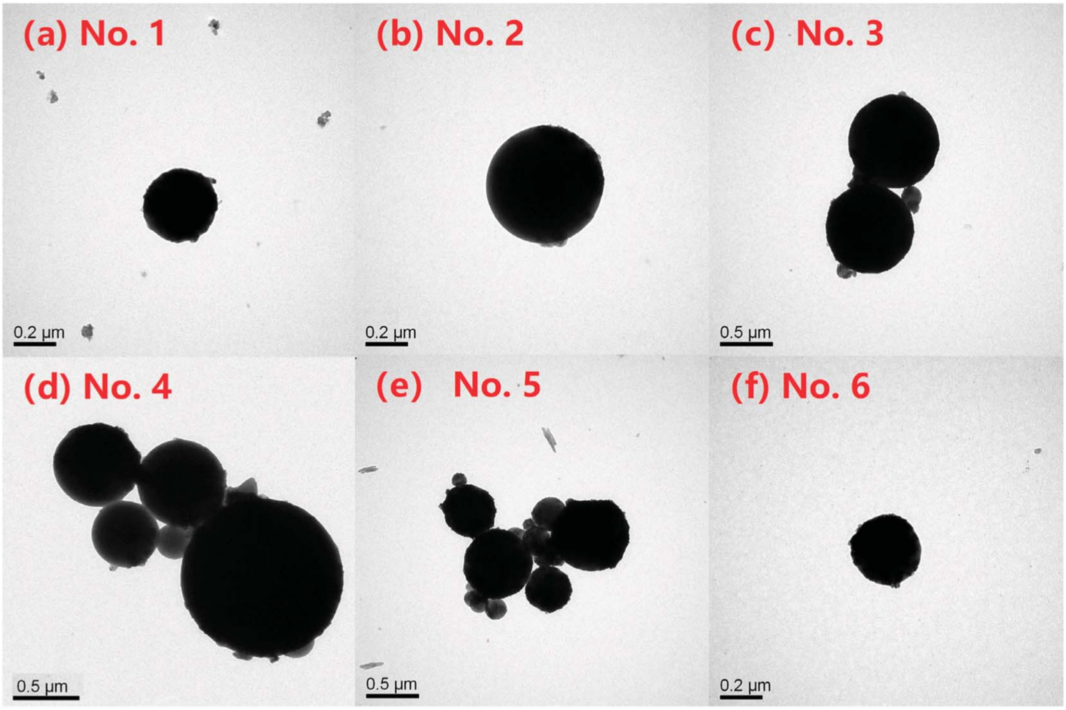

Fig. 1 TEM images of (a) no. 1 nFe_3O_4@IIP-D0-G8; (b) no. 2 nFe_3O_4@IIP-D0.5-G8; (c) no. 3 nFe_3O_4@IIP-D1-G8; (d) no. 4 nFe_3O_4@IIP-D2-G8; (e) no. 5 nFe_3O_4@NIP-D0.5-G8; (f) no. 6 nFe_3O_4.

volume of the ClO_4^- solution (mL), m is the adsorbent dosage (mg), the same hereinafter.

To investigate the effect of pH, 25 mL of 100 mg L^{-1} ClO_4^- with pH ranging from 2.0 to 10.0 were mixed with 20 mg of magnetic adsorbents for 1 h at 308 K, respectively. In the kinetic experiments, the nFe_3O_4@IIPs was also investigated with contacting time ranging from 1 to 180 min. The pseudo-first-order model (eqn (2)),[27] pseudo-second-order model (eqn (3)),[27,28] and intraparticle diffusion model (eqn (4)),[27] were used to fit the experimental data.

$$\log(q_e - q_t) = \log q_e - \left(\frac{k_1}{2.303}\right)t \tag{2}$$

$$\frac{t}{q_t} = \frac{1}{k_2 q_e^{\,2}} + \left(\frac{1}{q_e}\right)t \tag{3}$$

$$q_t = k_{id}t^{1/2} + C \tag{4}$$

where, q_e and q_t are the adsorption capacities at equilibrium and at time t (mg g^{-1}), respectively. k_1 (min^{-1}), k_2 (g (mg^{-1} min^{-1})) are the adsorption rate constants, k_{id} is the intraparticle diffusion rate constant (mg (g^{-1} $min^{-1/2}$)), C is the intercept (mg g^{-1}).

The adsorption isotherm studies were investigated with ClO_4^- initial concentration ranging from 0 to 500 mg L^{-1} at 308 K for 3 h. Two adsorption isotherms, Langmuir model (eqn (5))[27,29] and Freundlich model (eqn (6)) were applied to analyze the adsorption data[27,29]

$$\frac{C_e}{q_e} = \frac{1}{K_L q_m} + \frac{C_e}{q_m} \tag{5}$$

$$\log q_e = \log K_F + (1/n)\log C_e \tag{6}$$

where q_m and K_L are the Langmuir constants related to the maximum adsorption capacity and apparent heat change, respectively, while K_F is a Freundlich constant related to adsorption capacity and $1/n$ is a Freundlich constant related to the adsorption intensity.

2.5. Selectivity

Common ions with similar ionic radii of ClO_4^-, such as CrO_4^{2-}, $H_2PO_4^-$, NO_3^-, HSO_4^-, MnO_4^- and I^- were chosen to evaluate the selectivity of the nFe_3O_4@IIP and nFe_3O_4@NIP and individually dispersed into 25 mL of 100 mg L^{-1} ClO_4^-. The mixtures were shaken for 3 h at 308 K, and the concentrations of ClO_4^- and other ions in the supernatants were analyzed by ion chromatography (IC). The IL analysis was performed on a Thermo Scientific Dionex DX-500 with a gradient pump (Dionex GP50) at a flow of 0.25 mL min^{-1}, an autosampler (Dionex AS50) with 1000 μL-injection loop, a column thermostat set at 30 °C (Dionex Ultimate 3000 TCC-3000), an eluent generator (Dionex RFC-30) equipped with an eluent generator cartridge (Dionex EGC-III KOH), continuously regenerated trap column (Dionex CR-ATC), and a conductivity detector (Dionex CD-25). Separation was performed on a Dionex IonPac AS20 column and guard column-set. Columns and suppressor were in the 2 mm format, and data acquisition and evaluation were done using the Dionex Chromeleon 6.70 chromatography software. The eluent (35 mmol L^{-1} KOH) was produced electrolytically *in situ*. For eluent suppression prior to conductivity detection, a Dionex AERS 500 was used at a current setting of 22 mA. Samples were injected with volumes of 200 μL. The adsorptive amounts of ClO_4^- and other ions to nFe_3O_4@IIPs and nFe_3O_4@NIP were then compared.

The specific recognition properties of nFe_3O_4@IIPs are evaluated by imprinting factor (α), defined as eqn (7), and selectivity factor (β) defined as eqn (8):[30]

$$\alpha = \frac{q_{\mathrm{IIP}}}{q_{\mathrm{NIP}}} \tag{7}$$

where q_{IIP} and q_{NIP} are the adsorption capacity of the template or the analogue on IIP and NIP, respectively.

$$\beta = \frac{\alpha_{\mathrm{tem}}}{\alpha_{\mathrm{ana}}} \tag{8}$$

where, α_{tem} and α_{ana} are the imprinting factor toward the template ion and analogue, respectively.

3. Results and discussion

3.1. Characterization of nFe_3O_4@IIPs

The TEM spectra of the nFe_3O_4@IIPs were shown in Fig. 1. It revealed that the diameter of nFe_3O_4@IIPs increased from 200 nm to 800 nm with the increasing of the usage amount of DVB (Fig. 1(a)–(d)) during the co-polymerization procedure. It might be due to the fact that the more DVB used, the more cross-linking of polymer layer grafted onto the nFe_3O_4 magnetic core, which leading an increasing of the average diameter. When the usage amount of the DVB reached 1 g (Fig. 1(d)), the particle size distribution became not uniform and varied from 400 nm to 800 nm. The TEM spectra of the nFe_3O_4@NIP-D0.5-G8 (Fig. 1(e)) and nFe_3O_4 (Fig. 1(f)) were also investigated, and showed that the particle size distribution of the non-imprinted magnetic polymer was not as uniform as the imprinted analogues, ranging from 200–600 nm, while the bare nFe_3O_4 microspheres had a multidispersed spherical shape with a rough surface, with an average diameter of around 200 nm. The average diameter of the 4 kinds of nFe_3O_4@IIPs and the nFe_3O_4@NIP, as well as the bare nFe_3O_4 was summarized in Table 1.

The XRD of nFe_3O_4@IIPs was shown in Fig. 2. It indicated that nFe_3O_4@IIPs had retained the spinel structure of Fe_3O_4, in which the identical peaks for Fe_3O_4 located at 30.1°, 35.5°, 43.1°, 53.4°, 57.0° and 62.6°, corresponding to their indices (220), (311), (400), (422), (511) and (400) appeared.[31] The diffraction peaks of the nFe_3O_4@IIPs were slightly more broaden than that of pure nFe_3O_4. The FWHM of the peak at 35.5° (311) was taken as an example, increasing from 0.59933 (a, nFe_3O_4) to 0.64522 (b, nFe_3O_4@IIP-D0-G8); 0.65178 (c, nFe_3O_4@IIP-D0.5-G8); 0.69442 (d, nFe_3O_4@IIP-D1-G8); and 0.72884 (e, nFe_3O_4@IIP-D2-G8), which indicated that the nFe_3O_4@IIPs have smaller scale, which were consistent to the TEM results and might be favorable for the rapid adsorption and the increase of adsorption capacity.[31]

The paramagnetic property of the nFe_3O_4@IIPs was verified by the magnetization curve measured by VSM (Fig. 3). The saturation moments obtained from the hysteresis loops of were summarized in Table 1, and found to be at 35.6–42.8 emu g^{-1}, varying with the usage amount of DVB. The nFe_3O_4@IIPs was expected to respond well to magnetic field without any permanent magnetization, therefore making the solid and liquid phases separate easily. For comparing, the saturation moments, Fe_3O_4 contents and nitrogen contents of all the prepared nFe_3O_4@IIPs and nFe_3O_4@NIP were also investigated. Results were shown in Table 1. The Fe_3O_4 content of the nFe_3O_4@IIP decreased from 41.5% to 35.4% (no. 1 to 4 in Table 1) with the usage amount of the DVB increased during the preparation procedure. The results were consistent to the VSM results of the nFe_3O_4@IIPs. With the increasing of the usage amount of the DVB, the nonmagnetic sensitive polymer shell grafted onto the surface of the nFe_3O_4 increased, leading the Fe_3O_4 content of the nFe_3O_4@IIPs decreased as well as the saturation moments decreased. The nitrogen content of the nFe_3O_4@IIPs decreased from 7.82 to 7.08 mmol g^{-1}, with the usage amount of the DVB. With fixed usage amount of the GMA, the increasing the usage amount the DVB (no. 1 to 4 in Table 1) would cause a decrease of

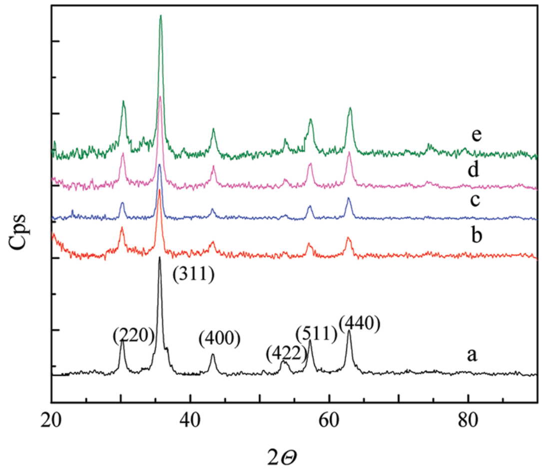

Fig. 2 The XRD of (a) nFe_3O_4; (b) nFe_3O_4@IIP-D0-G8; (c) nFe_3O_4@IIP-D0.5-G8; (d) nFe_3O_4@IIP-D1-G8; (e) nFe_3O_4@IIP-D2-G8.

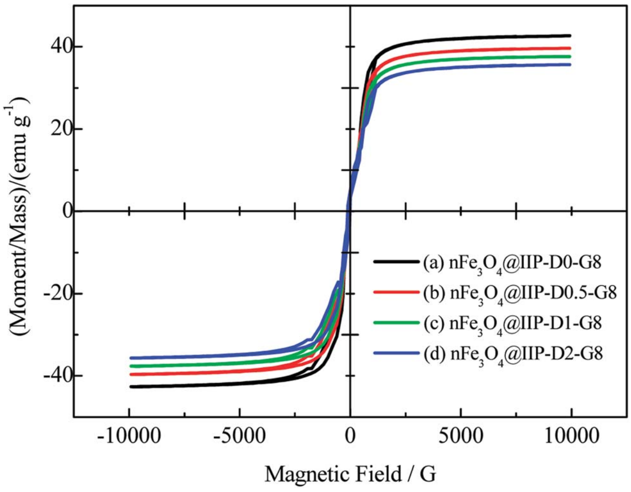

Fig. 3 The VSM of (a) nFe_3O_4@IIP-D0-G8; (b) nFe_3O_4@IIP-D0.5-G8; (c) nFe_3O_4@IIP-D1-G8; (d) nFe_3O_4@IIP-D2-G8.

the percentage of the GMA groups in polymer shell, thus leading a slight decrease of amino-groups *via* ring-opening reaction, and eventually leading a decrease of the nitrogen percentage (Table 1).

3.2. Effect of solution pH and the presumed adsorption mechanism

The adsorption capacity of the nFe_3O_4@NIP-D0.5-G8 and the nFe_3O_4@IIPs were investigated for the pH values ranging from 1.5 to 7.0. The results were shown in Fig. 4. The adsorption capacity of nFe_3O_4@NIP-D0-G8 to ClO_4^- was dependent on solution pH (Fig. 4(a)). With the solution pH increasing, the adsorption capacities firstly increased with the solution pH ranging from 1.5 to 3.0, and reached to the maximum at pH 3.0, then decreased. Those of the nFe_3O_4@IIPs were of similar trends. For the 4 kinds of nFe_3O_4@IIPs obtained with the usage of DVB varied (Fig. 4(b)–(e)), the highest adsorption capacities was obtained for the nFe_3O_4@IIP-D0.5-G8, while the lowest one was the nFe_3O_4@IIP-D2-G8, with almost 2 times of the adsorption capacities as that of nFe_3O_4@NIP-D0-G8. Except nFe_3O_4@IIP-D0-G8, this result was consistent with the nitrogen content of the nFe_3O_4@IIPs. The higher nitrogen content implied the more amino groups anchored on the surface of the nFe_3O_4@IIPs, leading a higher adsorption capacities, which was consistent to the results of the nitrogen percentage of the nFe_3O_4@IIPs, as discussed above and shown in Table 1. Interestingly, the solution pH affect the adsorption of the nFe_3O_4@IIP-D0-G8 much more significantly than the other nFe_3O_4@IIPs obtained *via* adding a certain amount of DVB. As shown in Fig. 4(b), with the solution pH increasing, the adsorption capacities of the nFe_3O_4@IIP-D0-G8 increased sharply and reached to the maximum at pH 3.0, then decreased sharply, as well. However, the adsorption capacities varying of the other nFe_3O_4@IIPs (Fig. 4(c)–(e)) was relatively much milder in the range of pH value 2–4. This implied that the presence of DVB might be contributed to the stabilization of ion imprinting holes, which would be favorable to the improvement of adsorption capacity and to the stabilization of a wider pH range.

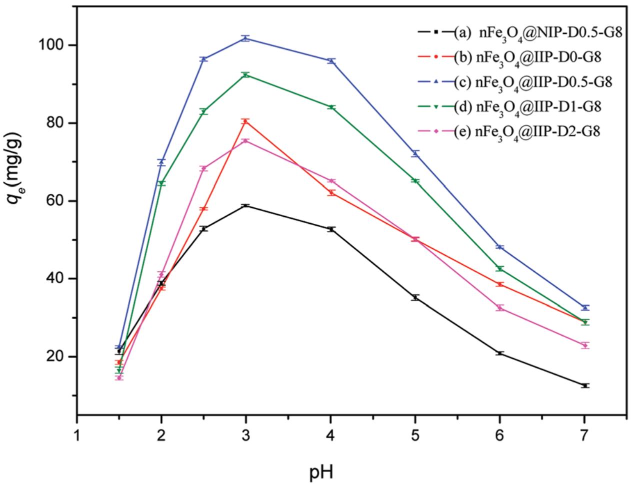

Fig. 4 Effect of solution pH value on the adsorption of ClO_4^- by nFe_3O_4@NIP-D-0.5-G8 (a), nFe_3O_4@IIPs (with DVB varied (b)–(e)).

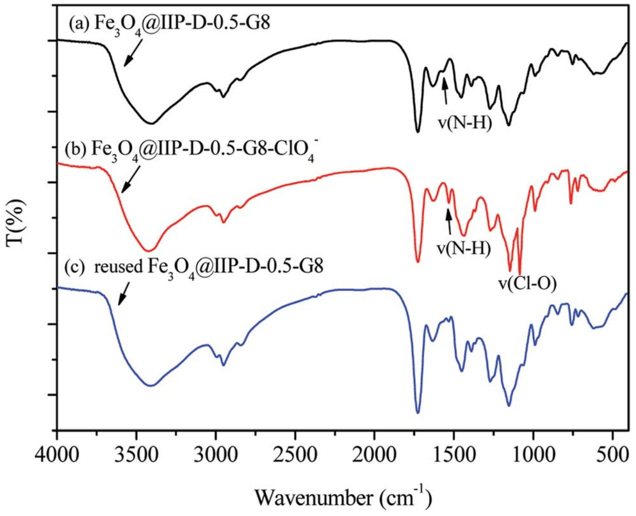

Fig. 5 FTIR of the nFe_3O_4@IIP-D-0.5-G8 (a) before, (b) after adsorption of ClO_4^- and (c) reused.

The FTIR spectra of nFe_3O_4@IIP-D-0.5-G8 before and after adsorption of ClO_4^- were showed in Fig. 5 and could be used for the confirmation of the adsorption mechanism. As shown in Fig. 5(a), the characteristic band of Fe_3O_4 occurred at $\sim$589 cm^{-1}. The broad peak appeared at $\sim$3400 cm^{-1} and 1635, $\sim$1568 cm^{-1} can be assigned to be the stretching and bending vibrations of the –OH, $-NH_2^+$ and $-NH_3^+$ groups. The stretching vibration absorptions of $-CH_2$ and $-CH_3$ appeared at $\sim$2924 cm^{-1}, $\sim$2853 cm^{-1}, while that of C=O appeared at $\sim$1630 cm^{-1}. After adsorption (Fig. 5(b)), the characteristic bands at $\sim$1568 cm^{-1} shifted to $\sim$1530 cm^{-1} along with the appearance of two new bands at $\sim$1090 cm^{-1} and $\sim$1145 cm^{-1}. After desorption (Fig. 5(c)), the latter two peaks disappeared, which might be attributed to the stretching vibration of the ClO_4^- (ref. 32), indicating that the interaction between $-NH_2^+$ and $-NH_3^+$ groups and the ClO_4^- were realized *via* the electrostatic interaction.

3.3. Kinetic studies

Fig. 6 presented the adsorption kinetics of ClO_4^-, onto nFe_3O_4@IIPs and nFe_3O_4@NIP. As shown in Fig. 6 (left, (a) and (b)), for nFe_3O_4@NIP-D-0.5-G8 and nFe_3O_4@IIP-D-0-G8, the adsorption capacity increased gradually and reached equilibrium in nearly 60 min, while for nFe_3O_4@IIP-D-0.5-G8, nFe_3O_4@IIP-D-1-G8 and nFe_3O_4@IIP-D-2-G8 (Fig. 6, left, (c)–(e), respectively), the adsorption capacity increased rapidly, and only 10 min were needed to reach adsorption equilibrium. This revealed that the existing of the ClO_4^--template and the presence of DVB for the crosslinking during the preparation process would stabilize the surface imprinting cavities in polymer matrix of the nFe_3O_4@IIPs and eventually shorten the equilibrium time. The kinetic curves of nFe_3O_4@NIP-D-0.5-G8 and nFe_3O_4@IIP-D-0-G8, could be divided into three portions, which could be described by intraparticle diffusion model (shown in

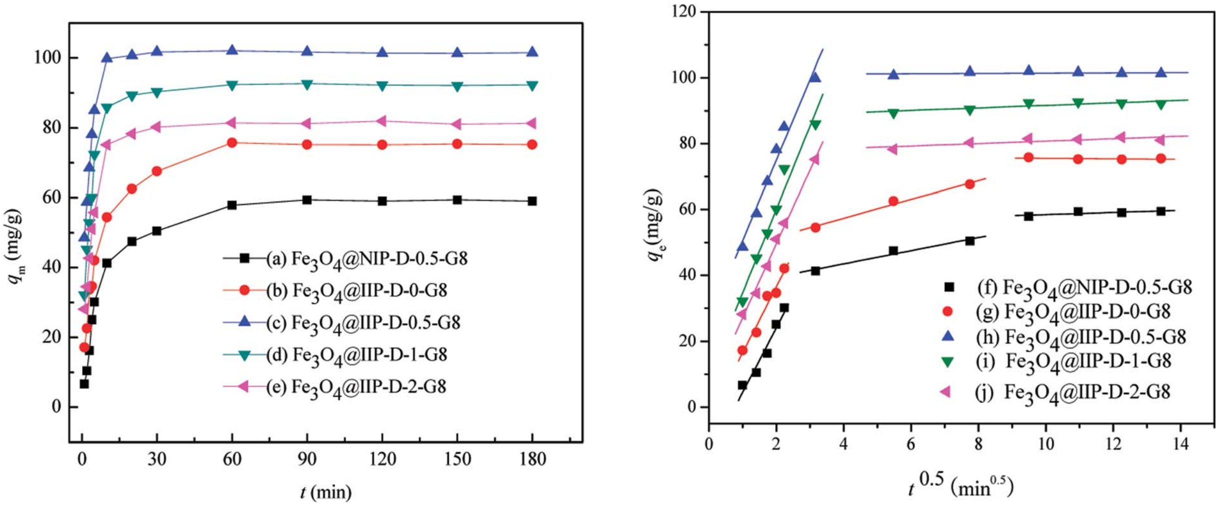

Fig. 6 Effect of adsorption time on the adsorption of ClO_4^- by nFe$_3$O$_4$@NIPs-D-0.5-G8 (a), (f), nFe$_3$O$_4$@IIPs (with DVB varied (b)–(e), (g)–(j)).

Fig. 6, right, (f) and (g)) and indicated that the intra-particle process[33] might be one of the rate-limiting steps for ClO_4^- removal. The kinetic curves of the other nFe$_3$O$_4$@IIPs could only be divided into two portions (Fig. 6, right, (h)–(j)), thus, the intra-particle process might not be involved in the rate-limiting steps. Therefore, in the present case, ClO_4^- reached the surface imprinting cavities of nFe$_3$O$_4$@IIPs easily and took less time to reach adsorption equilibrium, implying that the surface imprinting and uniform structures of nFe$_3$O$_4$@IIPs allowed efficient mass transport, thus overcoming some drawbacks of traditionally non-imprinting materials. The presence of DVB for the crosslinking took an important role for the stabilization of the imprinting cavities of the nFe$_3$O$_4$@IIPs and favorable for the adsorption kinetic processes.

Pseudo-first-order and pseudo-second-order models were used to describe the adsorption kinetic data. The results were shown in ESI, Fig. S1 and S2.‡ The correlation coefficient values indicated a better fit of the pseudo-second-order model with the experimental data compared to the pseudo-first-order for all the nFe$_3$O$_4$@IIPs and nFe$_3$O$_4$@NIP (Table 2). The calculated q_e values were in agreement with the theoretical ones, and the plots showed good linearity with R^2 above 0.999. Therefore, the adsorption behaviors followed the pseudo-second-order model, suggesting a chemisorption process,[34] including both ion exchange and electrostatic interaction.

3.4. Adsorption capacities

The adsorption capacities of ClO_4^- were investigated for all the nFe$_3$O$_4$@IIPs and nFe$_3$O$_4$@NIP (Fig. 7). Both Langmuir and Freundlich adsorption models were applied for data fitting analysis. The results were shown in ESI, Fig. S3 and S4.‡ The represented parameters using Langmuir and Freundlich adsorption models indicated that the Langmuir model could effectively describe the adsorption data with $R^2 > 0.995$ (Table 3), suggesting a better fit of the Langmuir isotherm rather than Freundlich isotherm, which suggested a monolayer adsorption.

As shown in Fig. 7(a) and Table 3, the maximum adsorption capacities of nFe$_3$O$_4$@IIPs ($q_{m,c} = 76.92$–111.1 mg g^{-1}; $q_{m,e} = 75.7$–108.9 mg g^{-1}) were much higher than that of nFe$_3$O$_4$@-NIPs-D-0.5-G8 ($q_{m,c} = 60.61$ mg g^{-1}; $q_{m,e} = 59.0$ mg g^{-1}). It can be seen that by using the ion imprinting technology, the adsorptive capacities of the obtained materials (nFe$_3$O$_4$@IIPs) to ClO_4^- can be improved. Although with the usage amount of the crosslinking agent DVB increased, the contents of the protonated amino groups in the nFe$_3$O$_4$@IIPs reduced 1.1%∼3.4% from nFe$_3$O$_4$@IIPs-D-0-G8 to nFe$_3$O$_4$@IIPs-D-2-G8 (Table 1), the adsorption capacities of the nFe$_3$O$_4$@IIPs did not decrease as expected, but an increase of around 34.6% for nFe$_3$O$_4$@IIP-D0.5-G8 and 16.2% for nFe$_3$O$_4$@IIP-D1-G8, were observed (Table 3). And till to the amount of DVB increased to 2.0 g, the decrease of the adsorption capacity at about 4.9%

Table 2 Pseudo-first-order and pseudo-second-order models and constants

		Pseudo-first-order model			Pseudo-second-order model		
Adsorbents	$q_{e,exp}$ (mg g^{-1})	k_1 (min^{-1})	$q_{e,cal}$ (mg g^{-1})	R^2	k_2 (g (mg^{-1} min^{-1}))	$q_{e,cal}$ (mg g^{-1})	R^2
nFe$_3$O$_4$@IIP-D0-G8	75.8	0.0689	24.7	0.6301	0.0032	77.5	0.9992
nFe$_3$O$_4$@IIP-D0.5-G8	102	0.052	7.58	0.3553	0.0122	102	0.9997
nFe$_3$O$_4$@IIP-D1-G8	92.7	0.735	13.7	0.532	0.0072	93.5	0.9999
nFe$_3$O$_4$@IIP-D2-G8	81.9	0.0619	16.14	0.6124	0.0067	82.6	0.9999
nFe$_3$O$_4$@NIP-D0.5-G8	59.5	0.081	28.77	0.8166	0.00243	62.5	0.9998

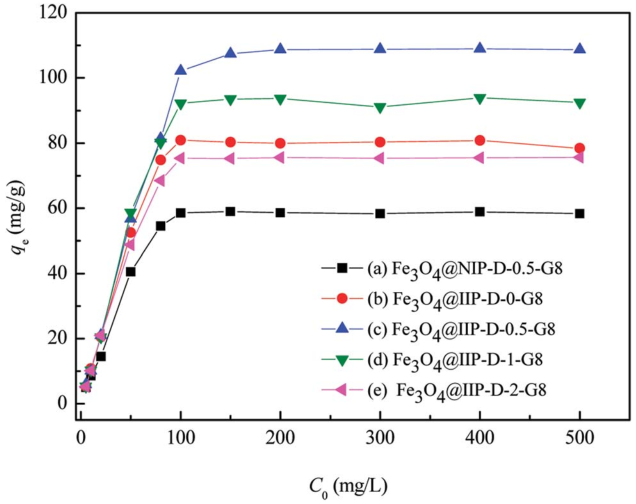

Fig. 7 Adsorption isotherm of ClO_4^- onto nFe_3O_4@NIPs-D-0.5-G8 (a) and nFe_3O_4@IIPs (with DVB varied (b)–(e)).

appeared for nFe_3O_4@IIP-D2-G8 (Table 3). It implied that the usage amount of DVB not only affected the structure of the material in the process of material synthesis, but also played a positive correlation with the adsorption properties of the material at a suitable usage amount. Too much amount of crosslinking agent DVB, 2.0 g in the present work, might cause the active site of the protonated amino group wrapped inside the polymer chain, thus reducing the adsorption capacity.

3.5. Adsorption selectivity

It is of great importance to assess the selective recognition towards the template for a novel imprinted material. Adsorption selectivity is known to be related to the size, shape, and functionality of the template of the imprinted cavities in imprinted materials.[16] Herein, the selectivity of nFe_3O_4@IIP-D0.5-G8 and nFe_3O_4@NIP-D0.5-G8 towards ClO_4^- and some other ions with similar ionic radii,[35] *i.e.*, CrO_4^{2-}, $H_2PO_4^-$, NO_3^-, HSO_4^-, MnO_4^- and I^- at individual concentration of 100 mg L^{-1} was studied. The imprinting factor (α) of nFe_3O_4@IIP-D0.5-G8 for ClO_4^{2-} was 1.8, which was much larger than those of the other ions with similar ionic radii (Table 4). The high selectivity factors (β) of the analogs (5.9–49.4) also exhibited high selectivity of nFe_3O_4@IIP-D0.5-G8 toward ClO_4^-. This could be attributed to the fact that in adsorbing process, specific recognition sites respect to template ion (here, *i.e.*, ClO_4^-) were generated on the surface of nFe_3O_4@IIP-D0.5-G8, thus ClO_4^- was strongly bound to the specific binding sites. As the competitive ions, the recognition sites of the imprinting cavities were not complementary to them, so it had less chance to be adsorbed on the nFe_3O_4@IIP-D0.5-G8. In contrast, the nFe_3O_4@NIP-D0.5-G8 adsorbed template much less than that of nFe_3O_4@IIP-D0.5-G8 since nFe_3O_4@NIP-D0.5-G8 had not generated specific recognition sites due to the absence of template ion.

Table 4 Imprinting factors (α) and selectivity factors (β) of Fe_3O_4@IIP(St–HPMA–DVB)-0.5 [a]

Ion	Ionic radius (aq.)/nm	q_{IIP} (mg g^{-1})	q_{NIP} (mg g^{-1})	α	β
ClO_4^-	0.240	111.1	60.6	1.8	
CrO_4^{2-}	0.240	28.5	122.5	0.2	7.7
$H_2PO_4^-$	0.238	22.1	72.5	0.3	5.9
NO_3^-	0.200	2.5	68.6	0.0	49.4
HSO_4^-	0.230	6.5	62.8	0.1	17.4
MnO_4^-	0.240	7.6	60.8	0.1	14.4
I^-	0.285	2.8	42.3	0.1	27.2

[a] q_{IIP}: Adsorption capacity of Fe_3O_4@IIP(St–HPMA–DVB)-0.5; q_{NIP}: adsorption capacity of Fe_3O_4@NIP(St–HPMA–DVB)-0.5; α: imprinting factor; β: the selectivity factor.

3.6. Reusability investigation

The reusable of the Fe_3O_4@IIPs was evaluated by comparing the adsorption efficiency. The ClO_4^- loaded Fe_3O_4@IIPs was extracted with 0.5 mol L^{-1} methanol/NaOH solution for 10 min twice, and then for adsorption to get the adsorption efficiency. Table 5 listed the reusability of Fe_3O_4@IIPs for ClO_4^-. The results indicated that nFe_3O_4@IIP-D0.5-G8 and nFe_3O_4@IIP-D1-G8 could be used for at least five cycles with a loss of less than 5% upon recovery on average, while desorption efficiencies decreased to 78.8–80.6%, and the re-adsorption capacities decreased to 43.4–45.5%, for nFe_3O_4@NIP-D0.5-G8, nFe_3O_4@IIP-D0-G8 and nFe_3O_4@IIP-D2-G8, which further implied that the usage amount of DVB played an important role for the stabilization of the active site of the protonated amino group and the imprinting cavities of the nFe_3O_4@IIPs when the usage amount at 0.5–1 g during the preparation procedure.

3.7. Adsorption comparison

The adsorption capacities of nFe_3O_4@IIPs and nFe_3O_4@NIP compared with other adsorbents examined for the removal of

Table 3 Langmuir and Freundlich isotherms and constants of ClO_4^- adsorption

		Langmuir isotherm			Freundlich isotherm		
Adsorbents	$q_{m,e}$ (mg g^{-1})	K_L (L mg^{-1})	$q_{m,c}$ (mg g^{-1})	R^2	K_F	$1/n$	R^2
nFe_3O_4@IIP-D0-G8	80.9	0.1105	83.33	0.9989	2.976	0.3827	0.7725
nFe_3O_4@IIP-D0.5-G8	108.9	0.1445	111.1	0.9987	3.269	0.4045	0.7854
nFe_3O_4@IIP-D1-G8	94.0	0.1537	95.24	0.9986	3.158	0.3852	0.694
nFe_3O_4@IIP-D2-G8	75.7	0.1593	76.92	0.9994	2.825	0.3915	0.7986
nFe_3O_4@NIP-D0.5-G8	59.0	0.0978	60.61	0.9977	2.349	0.4146	0.8310

Table 5 Reusability of Fe_3O_4@IIP(St–HPMA–DVB) for ClO_4^-

Adsorbent	Reusability[a] (%)	Run 1	Run 2	Run 3	Run 4	Run 5
nFe_3O_4@IIP-D0-G8	Des	95.1	90.6	89.0	82.4	80.6
	Ads	70.3	68.8	57.9	48.8	45.5
nFe_3O_4@IIP-D0.5-G8	Des	95.3	90.1	88.0	82.0	80.4
	Ads	72.3	69.7	56.4	48.6	44.5
nFe_3O_4@IIP-D1-G8	Des	99.1	99.6	99.0	98.4	98.6
	Ads	98.3	98.8	97.9	98.8	98.5
nFe_3O_4@IIP-D2-G8	Des	99.0	98.9	98.6	98.2	98.2
	Ads	97.5	98.3	97.9	97.4	97.9
nFe_3O_4@NIP-D0.5-G8	Des	93.9	90.3	86.8	80.8	78.8
	Ads	72.0	69.0	58.1	48.0	43.4

[a] Des: desorption efficiency (%); Ads: adsorption efficiency (%).

Table 6 Comparison of adsorption properties of different adsorbents ClO_4^-

Adsorbent	Functional group	Model	q_m/(mg g^{-1})	Ref.
Activated carbon	NA[a]	L[b], F[c],T[d]	8.04–13.00	36
Cationic surfactant loaded activated carbon	Cationic surfactant	NA[a]	21.14–29.59	8
Calcined Zn/Al layered double hydroxides	$-NR_4^+$	F[c]	NA[a]	37
nFe_3O_4@NIP-D0.5-G8	$-NH_2^+$, $-NH_3^+$	L[b]	60.6	This work
nFe_3O_4@IIP-D0-G8	$-NH_2^+$, $-NH_3^+$	L[b]	83.3	This work
nFe_3O_4@IIP-D0.5-G8	$-NH_2^+$, $-NH_3^+$	L[b]	111.1	This work
nFe_3O_4@IIP-D1-G8	$-NH_2^+$, $-NH_3^+$	L[b]	95.2	This work
nFe_3O_4@IIP-D2-G8	$-NH_2^+$, $-NH_3^+$	L[b]	76.9	This work

[a] NA: not available. [b] L: Langmuir. [c] F: Freundlich. [d] T: Tempkin.

ClO_4^- under similar conditions are summarized in Table 6. The results indicate that the as-prepared nFe_3O_4@IIPs in this work has 3.7–14 times of adsorption capacity as that of other adsorbents reported in the literature, and twice as that of the non-printed one, *i.e.*, nFe_3O_4@NIP-D0.5-G8. Hence, the newly developed nFe_3O_4@IIPs has promising potential applications in the removal of ClO_4^- from environmental water.

4. Conclusion

A series of novel protonated amino functionalized core–shell ionic imprinted magnetic polymers (nFe_3O_4@IIPs) was controlled prepared by ultrasonic assisted suspension polymerization and surface imprinting technique. The as-prepared nFe_3O_4@IIPs exhibited a homogeneous morphology, highly selective recognition, strong affinity ability, and high magnetic responsiveness for the adsorption of ClO_4^- in aqueous. The adsorption mechanism of the ClO_4^- onto the nFe_3O_4@IIPs is mainly related to ion exchange and electrostatic attraction, in which the protonated amino groups and imprinting cavities play a cooperative role in the adsorption of ClO_4^-.

Conflicts of interest

There are no conflicts to declare.

Acknowledgements

We would like to thank the National Natural Science Foundation of China (51608479), the National Natural Science Foundation of Zhejiang Province (LY14B04003), the National Natural Science Foundation of Ningbo (2014A610092), the National College Students' innovation and entrepreneurship training program (201713022009), the Xinmiao Students' innovation training program of Zhejiang Province (2017R401181) for the financial support.

References

1 L. Yao, L. X. Yang, J. M. Chen, K. Toda, X. F. Wang, J. M. Zhang, D. Yamasaki, Y. Nakamura, X. Sui, L. F. Zheng, L. Wen, C. H. Xu and W. X. Wang, Levels, indoor-outdoor relationships and exposure risks of airborne particle-associated perchlorate and chlorate in two urban areas in Eastern Asia, *Chemosphere*, 2015, **135**, 31–37.

2 V. I. Furdui, J. C. Zheng and A. Furdui, Anthropogenic Perchlorate Increases since 1980 in the Canadian High Arctic, *Environ. Sci. Technol.*, 2018, **52**, 972–981.

3 W. A. Jackson, S. X. Wang, B. Rao, T. Anderson and N. L. Estrada, Heterogeneous Production of Perchlorate and Chlorate by Ozone Oxidation of Chloride: Implications on the Source of (Per)Chlorate in the Solar System, *Environ. Sci. Technol.*, 2018, **2**, 87–94.

4 P. Kumarathilaka, C. Oze, S. P. Indraratne and M. Vithanage, Perchlorate as an emerging contaminant in soil, water and food, *Chemosphere*, 2016, **150**, 667–677.

5 J. A. Carr, S. Murali, F. Hua, W. L. Goleman, D. L. Carr, E. E. Smith and M. Wages, Changes in gastric sodium-iodide symporter (NIS) activity are associated with differences in thyroid gland sensitivity to perchlorate during metamorphosis, *Gen. Comp. Endocrinol.*, 2015, **219**, 16–23.

6 R. Epsztein, C. Desitti, M. Beliavski, S. Tarre and M. Green, Co-reduction of nitrate and perchlorate in a pressurized hydrogenotrophic reactor with complete H-2 utilization, *Chem. Eng. J.*, 2017, **328**, 133–140.

7 M. C. Gao, S. Wang, Y. Ren, C. J. Jin, Z. L. She, Y. G. Zhao, S. Y. Yang, L. Guo, J. Zhang and Z. W. Li, Simultaneous removal of perchlorate and nitrate in a combined reactor of sulfur autotrophy and electrochemical hydrogen autotrophy, *Chem. Eng. J.*, 2016, **284**, 1008–1016.

8 S. Y. Lin, W. F. Chen, M. T. Cheng and Q. Li, Investigation of factors that affect cationic surfactant loading on activated carbon and perchlorate adsorption, *Colloids Surf., A*, 2013, **434**, 236–242.

9 X. M. Wu, Y. L. Wang, L. L. Xu and L. Lv, Removal of perchlorate contaminants by calcined Zn/Al layered double hydroxides: equilibrium, kinetics, and column studies, *Desalination*, 2010, **256**, 136–140.

10 Y. H. Xie, S. Y. Li, F. Wang and G. L. Liu, Removal of perchlorate from aqueous solution using protonated cross-linked chitosan, *Chem. Eng. J.*, 2010, **156**, 56–63.

11 H. G. Zhang, T. Li, Z. Q. Yang, M. H. Su, L. Hou, D. Y. Chen and D. G. Luo, Highly efficient removal of perchlorate and phosphate by tailored cationic metal-organic frameworks based on sulfonic ligand linking with Cu-4,4′-bipyridyl chains, *Sep. Purif. Technol.*, 2017, **188**, 293–302.

12 K. D. Hurley and J. R. Shapley, Efficient heterogeneous catalytic reduction of perchlorate in water, *Environ. Sci. Technol.*, 2007, **41**, 2044–2049.

13 R. Mahmudovr, Y. Shu, S. Rykov, J. G. Chen and C. P. Huang, The reduction of perchlorate by hydrogenation catalysts, *Appl. Catal., B*, 2008, **81**, 78–87.

14 Z. Xiong, D. Y. Zhao and G. Pan, Rapid and complete destruction of perchlorate in water and ion-exchange brine using stabilized zero-valent iron nanoparticles, *Water Res.*, 2007, **41**, 3497–3505.

15 D. L. Wu, P. He, X. H. Xu, M. Zhou, Z. Zhang and Z. Houda, The effect of various reaction parameters on bioremediation of perchlorate-contaminated water, *J. Hazard. Mater.*, 2008, **150**, 419–423.

16 J. Q. Fu, L. X. Chen, J. H. Li and Z. Zhang, Current status and challenges of ion imprinting, *J. Mater. Chem. A*, 2015, **3**, 13598–13627.

17 R. Gil, C. G. Amorim, L. Crombie, P. K. T. Lin, A. Araffljo and M. C. Montenegro, Study of a Novel Bisnaphthalimidopropyl Polyamine as Electroactive Material for Perchlorate-selective Potentiometric Sensors, *Electroanalysis*, 2015, **27**, 2809–2819.

18 X. Zuo, D. Mosha, S. J. Archibald, A. K. McCasland, A. M. Hassan, R. S. Givens and D. H. Busch, Toward the soil poultice and a new separations methodology: Rebinding of macrocyclic metal complexes to molecularly imprinted polymers specifically templated *via* noncovalent interactions, *J. Coord. Chem.*, 2005, **58**, 21–39.

19 T. S. Anirudhan and J. C. Binusreejayan, pH and magnetic field sensitive folic acid conjugated protein-polyelectrolyte complex for the controlled and targeted delivery of 5-fluorouracil, *J. Ind. Eng. Chem.*, 2018, **57**, 199–207.

20 M. E. Mahmoud, A. A. Yakout, K. H. Hamza and M. M. Osman, Novel nano-Fe_3O_4-encapsulated-dioctylphthalate and linked-triethylenetetramine sorbents for magnetic solid phase removal of heavy metals, *J. Ind. Eng. Chem.*, 2015, **25**, 207–215.

21 A. Magdy, Y. O. Fouad, M. H. Abdel-Aziz and A. H. Konsowa, Synthesis and characterization of Fe_3O_4/kaolin magnetic nanocomposite and its application in wastewater treatment, *J. Ind. Eng. Chem.*, 2017, **56**, 299–311.

22 S. D. Pan, H. Y. Shen, Q. H. Xu, J. Luo and M. Q. Hu, Surface mercapto engineered magnetic Fe_3O_4 nanoadsorbent for the removal of mercury from aqueous solutions, *J. Colloid Interface Sci.*, 2012, **365**, 204–212.

23 H. Y. Shen, Z. X. Chen, Z. H. Li, M. Q. Hu, X. Y. Dong and Q. H. Xia, Controlled synthesis of 2,4,6-trichlorophenol-imprinted amino-functionalized nano-Fe_3O_4-polymer magnetic composite for highly selective adsorption, *Colloids Surf., A*, 2015, **481**, 439–450.

24 Y. Wang, S. Ye, S. S. Lv, J. L. Zhang and X. S. Ye, Preparation of ion imprinted Fe_3O_4@IIP(MMA–HPMA–DVB) magnetic composite and its selective adsorption to Ni(II), *Acta Mater. Compositae Sin.*, 2017, **34**, 2846–2855.

25 X. Q. Li, L. Fang, M. N. Zhang and Y. D. Liu, Measurement of Perchlorate Concentration in Groundwater Using Methylene Blue Complexation- Spectrophotometry, *Environ. Sci. Technol.*, 2014, **37**, 96–99.

26 H. Y. Shen, S. D. Pan, Y. Zhang, X. L. Huang and H. X. Gong, A New Insight on the Adsorption Mechanism of Amino-functionalized Nano-Fe_3O_4 Magnetic Polymers in Cu(II), Cr(VI) Co-existing Water System, *Chem. Eng. J.*, 2012, **183**, 180–191.

27 J. Febrianto, A. N. Kosasih, J. Sunarso, Y. H. Ju, N. Indraswati and S. Ismadji, Equilibrium and kinetic studies in adsorption of heavy metals using biosorbent: A summary of recent studies, *J. Hazard. Mater.*, 2009, **162**, 616–645.

28 Y. S. Ho, Review of second-order models for adsorption systems, *J. Hazard. Mater.*, 2006, **136**, 681–689.

29 S. H. Huang and D. H. Chen, Rapid removal of heavy metal cations and anions from aqueous solutions by an amino-functionalized magnetic nano-adsorbent, *J. Hazard. Mater.*, 2009, **163**, 174–179.

30 W. Zhang, L. Qin, X. W. He, W. Y. Li and Y. K. Zhang, Novel surface modified molecularly imprinted polymer using acryloyl-β-cyclodextrin and acrylamide as monomers for selective recognition of lysozyme in aqueous solution, *J. Chromatogr. A*, 2009, **1216**, 4560–4567.

31 Y. G. Zhao, H. Y. Shen, S. D. Pan, M. Q. Hu and Q. H. Xia, Preparation and characterization of amino-functionalized

nano-Fe_3O_4 magnetic polymer adsorbents for removal of chromium(VI) ions, *J. Mater. Sci.*, 2010, **49**, 5291–5301.

32 C. Liu and X. W. Lv, Identification of explosives by infrared spectroscopy, *Chem. Propellants Polym. Mater.*, 2017, **15**, 82–84.

33 K. Y. Foo and B. H. Hameed, Review: insights into the modeling of adsorption isotherm systems, *Chem. Eng. J.*, 2010, **156**, 2–10.

34 M. Q. Hu, H. Y. Shen, Z. H. Jiang, Y. F. Wang, L. Y. Wang and Q. Jiang, One-pot solvothermal preparation of ethylenediamine-functionalized nanochain and its adsorption-*in situ* degradation of 2,4,6-trichlorophenol, *Desalin. Water Treat.*, 2018, **102**, 253–263.

35 M. C. Simoes, K. J. Hughes, D. B. Ingham, L. Ma and M. Pourkashanian, Estimation of the Thermochemical Radii and ionic volumes of Complex Ions, *Inorg. Chem.*, 2017, **56**, 7566–7573.

36 N. Lu, N. Y. Gao and X. Huang, Adsorption of Perchlorate in Water by Granular Activated Carbon and Impact Factors Analysis, *Environ. Sci.*, 2008, **29**, 1572–1577.

37 Y. X. Wu, Y. W. Cheng, C. G. Hubbard, S. Hubbarda and J. B. Ajo-Frankli, Biogenic sulfide control by nitrate and (per)chlorate – A monitoring and modeling investigation, *Chem. Geol.*, 2018, **476**, 180–190.